Research Article

INTERNATIONAL JOURNAL OF ADVANCED ROBOTIC SYSTEMS

International Journal of Advanced Robotic Systems
September-October 2018: 1–15

DOI: 10.1177/1729881418800885
journals.sagepub.com/home/arx
SAGE

Model-free control of a quadrotor using adaptive proportional derivative-sliding mode control and robust integral of the signum of the error

Zhi Li, Xin Ma and Yibin Li

Abstract

In this article, a robust model-free trajectory tracking control strategy is developed for a quadrotor in the presence of external disturbances. The proposed strategy has an outer-inner-loop control structure. The outer loop controls the position with adaptive proportional derivative-sliding mode control and generates the desired attitude angles for the inner loop corresponding to the given position, velocity, and heading references, while the robust integral of the signum of the error method is applied to the inner loop to guarantee fast convergence of attitude angles. Asymptotic tracking of the three-dimensional trajectories is proven by the Lyapunov stability theory. The effectiveness of the proposed controller is demonstrated with the simulation results by comparing with other model-free quadrotor trajectory tracking controllers.

Keywords

Quadrotor, model-free, APD-SMC, RISE, trajectory tracking

Date received: 9 April 2018; accepted: 11 August 2018

Topic: Field Robotics
Topic Editor: Andrey V Savkin
Associate Editor: Yongping Pan

Introduction

Due to vertical take-off/landing capability, flight flexibility, and hovering stability, quadrotor unmanned aerial vehicles (UAVs) have attracted increasing attention in the past decades and have been widely used in surveillance, search and rescue, and so on.[1,2]

Trajectory tracking control of a quadrotor UAV is a challenging problem because of its nonlinear, strongly coupled, and underactuated dynamics. Moreover, the quadrotor system is susceptible to external disturbances such as wind, payload variations, and nonlinear frictions.[3,4]

Significant efforts have been made, and various control methods have been developed for the trajectory tracking control of quadrotor UAVs. The control methods can be divided into linear control methods such as proportional derivative (PD),[5–8] proportional integral derivative (PID),[9] linear quadratic regulation (LQR)[10]; nonlinear control methods such as backstepping,[11,12] sliding mode control (SMC),[13–16] model-free control (MFC),[17,18] adaptive control[19–21]; and intelligent control methods such as fuzzy control[22–24] and learning-based control.[25,26] These controllers could achieve satisfactory performances for attitude or position tracking of quadrotor UAVs in some circumstances. Kendoul[4] designed a PD^2 feedback controller for asymptotic attitude tracking of a quadrotor UAV. Pounds et al.[9] designed a PID controller for position and attitude stabilization of a quadrotor in the presence of load

Center for Robotics, School of Control Science and Engineering, Shandong University, Jinan, China

Corresponding author:
Xin Ma, Center for Robotics, School of Control Science and Engineering, Shandong University, 17923 Jingshi Road, Jinan, Shandong 250061, China.
Email: maxin@sdu.edu.cn

variation. Panomrattanarug et al.[10] designed an LQR-based attitude tracking controller in which the state variables are estimated using a full-order state observer. These linear controllers can stabilize the quadrotor's position and attitude only around the operation point, whereas they cannot achieve the desired stability and tracking trajectories in a large operation range and have limited capability to alleviate the coupling among state variables.

Nonlinear control methods that can overcome the limitations of linear control approaches have been widely used in controlling quadrotors. Taking into account the input saturation, An et al.[11] designed a backstepping inverse optimal attitude controller that has the maximum convergence rate Derafa et al.[13] developed a second-order super twisting sliding mode controller (STSMC) for the attitude tracking control of a quadrotor to ensure robustness to modeling errors and wind perturbations. Their works focus on the attitude tracking problem while position trajectory tracking control is also very important in practical applications. In consideration of quadrotor actuator effectiveness loss, the trajectory tracking problem is treated using a nonlinear disturbance observer–based resilient backstepping controller.[12] An SMC is designed for autonomous flight control of a quadrotor to ensure the position and yaw angle reach to the desired values asymptotically.[14] Furthermore, a terminal SMC is designed to make the quadrotor reach to the state of equilibrium in finite time in the presence of unexpected disturbances.[15] Considering that the onboard altitude sensors (barometer, global positioning system, etc.) do not provide the altitude velocity information, a high-order sliding mode observer is designed to estimate the altitude velocity. Based on the estimations, an STSMC is designed to address the quadrotor altitude tracking problem.[16] However, the backstepping[11,12] and SMCs[13–16] need good knowledge of the system dynamics, while the precise dynamic models of small quadrotor UAVs are very difficult to be obtained due to high coupling, uncertainties, and external disturbances.[27]

Without the requirement of the dynamic model, the MFC is a preferred remedy in which only the system input and output are needed to estimate the local model.[17] Combining the MFC with the terminal SMC, a model-free terminal sliding mode controller (MFTSMC) is designed to control the attitude and the position of a quadrotor UAV.[18] The time-delay-estimation-based MFC ensures bounded tracking errors, while the terminal SMC eliminates the bounded error in a finite time. However, the estimated model of the MFC is valid only in a short period and needs to be updated in every iteration, and the control gains are not easy for tuning. Other model independent controllers have been designed. Adaptive control that is suitable to solve the parametric uncertainty problem has been utilized for trajectory tracking of a quadrotor in the presence of parametric uncertainties.[19] However, the classic adaptive control requires the linear parameterization of nonlinear dynamics, while nonparametric uncertainties usually lead to performance degradation.[28] Torres et al.[22] designed a fuzzy feedback controller in which a distributed compensator is designed to stabilize the quadrotor. In the study by Gautam and Ha,[23] the PID controller is combined with the fuzzy logic to address the quadrotor attitude and position control problem. The PID gains are tuned using a self-tuning fuzzy algorithm, whereas the fuzzy parameters are achieved based on an extended Kalman filter. In the study by Kayacan and Maslim,[24] a type-2 fuzzy neural network position controller is combined with the traditional PD attitude controller to solve the trajectory tracking problem of a quadrotor in the presence of disturbance and uncertainties. Lou and Guo[26] used reinforcement learning method for trajectory tracking of a quadrotor, while policy-searching algorithm is applied to adjust the model parameters and compensate for disturbances. Due to the strong learning abilities, the intelligent controllers have achieved good performance in quadrotor trajectory tracking.[22–26] However, the intelligent controllers usually require high hardware conditions, which prevent their practical applications in low-cost quadrotors.

Recently, some simple MFC methods such as robust integral of the signum of the error (RISE)[29] and PD-SMC[30,31] have been proposed for trajectory tracking. The RISE controller can compensate for the disturbances and model uncertainties and ensure semiglobal asymptotic stability. It is applied for disturbance rejection in the inner loop of quadrotors.[32] In Shin et al.'s study,[33] neural network feedforward term is added to the RISE method to improve the attitude and altitude tracking performance of a rotorcraft. In the study by Yue et al.,[34] the PD-SMC method that combines the advantages of PD control and SMC has been applied in the contour tracking control of robotic manipulators to improve tracking performance.

Motivated by the requirement for the simple controller which has strong robustness to external disturbances and can be implemented easily in practical applications, this article proposes a model-free hierarchical controller scheme for trajectory tracking of a quadrotor UAV. The proposed control scheme has an outer-inner-loop structure. First, a model-free adaptive proportional derivative-sliding mode control (APD-SMC) law is proposed for the outer loop to make the quadrotor UAV track the desired position trajectory in which adaptive laws is used to estimate the upper bounds of the unknown terms. The APD-SMC enables the quadrotor to achieve null steady-state error tracking capability with reasonable control gains so that the need for large control gains of PD-SMC to compensate for disturbances is avoided. Second, the boundary layer method is used to eliminate chattering of the APD-SMC. A tracking differentiator is utilized to compute the desired attitude angular velocity which is needed for the inner loop controller to overcome the infinity problem caused by taking the derivative of the desired attitude angles. Third, to meet the requirement for fast response of attitude tracking control, the RISE method is employed in the inner loop for disturbance rejection and ensures locally exponentially

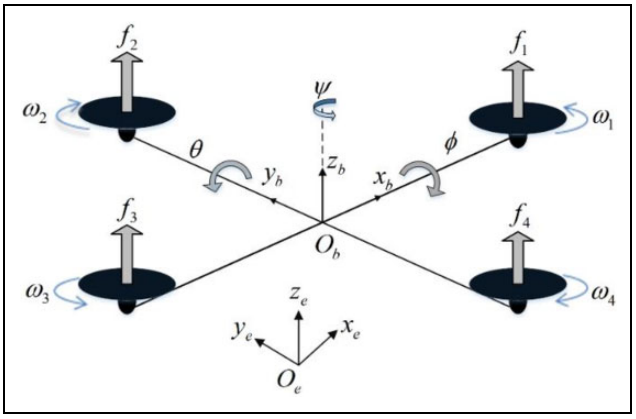

Figure 1. Schematic of a quadrotor.

Table 1. Description of the quadrotor UAV parameters.[37]

Symbol	Description	Value
m	Mass of the quadrotor	0.65 (kg)
l	Distance from the mass center to motors	0.2 (m)
k_c	Force-to-moment scaling factor	3.1×10^{-7} (N m s^2/rad^2
g	Gravitational acceleration	9.81(m/s^2)
J_x, J_y	Inertia moments about x and y axis	7.5×10^{-3}(kg m^2)
J_z	Inertia moments about z axis	1.3×10^{-2} (kg m^2)
$K_{\xi 1}$, $K_{\xi 2}$, $K_{\xi 3}$	Aerodynamic damping coefficients	0.01 (N s/m)

UAV: unmanned aerial vehicle.

stability of the inner loop. Finally, the asymptotic convergence of 3-D trajectory tracking of the quadrotor UAV is proved by using the Lyapunov stability theory.

This article is organized as follows. The dynamic model of a quadrotor UAV is given in the second section. The details of the hierarchical MFC design and stability analysis are presented in the third section. The comparison simulation experiments of the proposed controller with other MFCs are given in the fourth section. The final section concludes the article.

Dynamic model description

The schematic of a quadrotor UAV is shown in Figure 1. The quadrotor has four rotors mounted at two orthogonal directions. Rotors 1 and 3 rotate in the anticlockwise direction; rotors 2 and 4 rotate in the clockwise direction. The four thrusts (f_i, $i = 1, 2, 3, 4$) are generated by the rotation of the four rotors. The thrust is proportional to the square of the rotor's angular speed[35,36]

$$f_i = k_T \omega_i^2, \quad i = 1, 2, 3, 4 \tag{1}$$

where the thrust coefficient k_T depends on the blade rotor characteristics.

The control inputs u, τ_1, τ_2, and τ_3 can be obtained through the thrusts

$$\begin{bmatrix} u \\ \tau_1 \\ \tau_2 \\ \tau_3 \end{bmatrix} = \begin{bmatrix} 1 & 1 & 1 & 1 \\ 0 & d & 0 & -d \\ -d & 0 & d & 0 \\ -k_c & k_c & -k_c & k_c \end{bmatrix} \begin{bmatrix} f_1 \\ f_2 \\ f_3 \\ f_4 \end{bmatrix} \tag{2}$$

where u is the total thrust; τ_1, τ_2, and τ_3 are roll, pitch, and yaw control torques respectively; d is the distance from mass center to each rotor; and k_c is the force-to-moment scaling factor. The descriptions and values of the quadrotor UAV physical parameters are given in Table 1.

As shown in Figure 1, $(O_b - x_b y_b z_b)$ is the body-frame coordinates and $(O_e - x_e y_e z_e)$ is the earth-frame coordinates. The quadrotor UAV has six degree-of-freedom (DOF) motion, which includes the translational motion in three directions ($\xi = [x, \ y, \ z]^T$) and the rotational motion around three axes ($\eta = [\phi, \ \theta, \ \psi]^T$). The rotation matrix $R^{B \to E}$ describes the linear velocity relationship between $(O_b - x_b y_b z_b)$ and $(O_e - x_e y_e z_e)$. The transformation matrix $R_a^{B \to E}$ describes the angular velocity relationship between $(O_b - x_b y_b z_b)$ and $(O_e - x_e y_e z_e)$. $R^{B \to E}$ and $R_a^{B \to E}$ are given as

$$R^{B \to E} = \begin{bmatrix} c\theta c\psi & s\phi s\theta c\psi - c\phi s\psi & c\phi s\theta c\psi + s\phi s\psi \\ c\theta s\psi & s\phi s\theta s\psi + c\phi c\psi & c\phi s\theta s\psi - s\phi c\psi \\ -s\theta & s\phi c\theta & c\phi c\theta \end{bmatrix}$$
$$R_a^{B \to E} = \begin{bmatrix} 1 & s\phi t\theta & c\phi t\theta \\ 0 & c\phi & -s\phi \\ 0 & s\phi / c\theta & c\phi / c\theta \end{bmatrix} \tag{3}$$

where $c\cdot$, $s\cdot$, and $t\cdot$ represent $\cos(\cdot)$, $\sin(\cdot)$, and $\tan(\cdot)$, respectively.

Assuming that the quadrotor UAV is a rigid body and it is symmetric around the center of gravity, its dynamic model can be expressed with Newton–Euler formalism

$$\begin{cases} m\ddot{\xi} + K_\xi \dot{\xi} + mge + d_\xi = R^{B \to E} eu \\ M(\eta)\ddot{\eta} + C(\eta, \dot{\eta})\dot{\eta} - d_\eta = \tau \end{cases} \tag{4}$$

where $e = [0, 0, 1]^T$. $\tau = [\tau_1, \tau_2, \tau_3]^T$ denotes the rotational torque input. $d_\xi = [d_{\xi 1}, \ d_{\xi 2}, \ d_{\xi 3}]^T$ and $d_\eta = [d_{\eta 1}, \ d_{\eta 2}, \ d_{\eta 3}]^T$ represent the unknown disturbances. $K_\xi = \mathrm{diag}(K_{\xi 1}, K_{\xi 2}, K_{\xi 3})$ is the aerodynamic damping matrix. $M(\eta)$ acts as the inertia matrix for the full rotational kinetic energy of the rotorcraft expressed in terms of the generalized coordinates η. $C(\eta, \dot{\eta})$ is the Coriolis matrix which contains the gyroscopic and centrifugal terms associated with the η dependence of $M(\eta)$. $M(\eta)$ and $C(\eta, \dot{\eta})$ are defined as follows[38]

$$M(\eta) = \left((R_a^{B\to E})^{-1}\right)^T J (R_a^{B\to E})^{-1} = \begin{bmatrix} J_x & 0 & -J_x s\theta \\ 0 & J_y c^2\phi + J_z s^2\phi & (J_y - J_z)c\phi s\phi c\theta \\ -J_x s\theta & (J_y - J_z)c\phi s\phi c\theta & J_x s^2\theta + J_y s^2\phi c^2\theta + J_z c^2\phi c^2\theta \end{bmatrix} \tag{5}$$

and

$$C(\eta, \dot{\eta}) = \begin{bmatrix} C_{11} & C_{12} & C_{13} \\ C_{21} & C_{22} & C_{23} \\ C_{31} & C_{32} & C_{33} \end{bmatrix} \tag{6}$$

where $J = \mathrm{diag}(J_x,\ J_y,\ J_z)$ is the inertia moments matrix. C_{ij} $(i,j = 1, 2, 3)$ are given as follows

$$\begin{aligned} C_{11} &= 0 \\ C_{12} &= (J_y - J_z)(\dot{\theta}c\phi s\phi + \dot{\psi}s^2\phi c\theta) + (J_z - J_y)\dot{\psi}c^2\phi c\theta - J_x\dot{\psi}c\theta \\ C_{13} &= (J_z - J_y)\dot{\psi}c\phi s\phi c^2\theta \\ C_{21} &= (J_z - J_y)(\dot{\theta}c\phi s\phi + \dot{\psi}s^2\phi c\theta) + (J_y - J_z)\dot{\psi}c^2\phi c\theta + J_x\dot{\psi}c\theta \\ C_{22} &= (J_z - J_y)\dot{\phi}c\phi s\phi \\ C_{23} &= -J_x\dot{\psi}s\theta c\theta + J_y\dot{\psi}s^2\phi c\theta s\theta + J_z\dot{\psi}c^2\phi s\theta c\theta \\ C_{31} &= (J_y - J_z)\dot{\psi}c^2\theta s\phi c\phi - J_x\dot{\theta}c\theta \\ C_{32} &= (J_z - J_y)(\dot{\theta}c\phi s\phi s\theta + \dot{\phi}s^2\phi c\theta) + (J_y - J_z)\dot{\phi}c^2\phi c\theta \\ &\quad + J_x\dot{\psi}s\theta c\theta - J_y\dot{\psi}s^2\phi s\theta c\theta - J_z\dot{\psi}c^2\phi s\theta c\theta \\ C_{33} &= (J_y - J_z)\dot{\phi}c\phi s\phi c^2\theta - J_y\dot{\theta}s^2\phi c\theta s\theta - J_z\dot{\theta}c^2\phi c\theta s\theta + J_x\dot{\theta}c\theta s\theta \end{aligned} \tag{7}$$

Remark 1. The attitude angles ϕ and θ are bounded as $\phi \in \left(-\frac{\pi}{2}, \frac{\pi}{2}\right)$ and $\theta \in \left(-\frac{\pi}{2}, \frac{\pi}{2}\right)$.

Assumption 1. The unknown time-varying disturbances d_η and d_ξ are bounded and the derivative of d_η is also bounded.

Assumption 2. The state variables $\xi(t)$ and $\eta(t)$ and their derivatives $\dot{\xi}(t)$ and $\dot{\eta}(t)$ are measurable.

The desired position and desired attitude are $\xi_d(t) = [x_d(t),\ y_d(t),\ z_d(t)]^T$ and $\eta_d(t) = [\phi_d(t),\ \theta_d(t),\ \psi_d(t)]^T$, respectively. The tracking errors are defined as

$$E_\xi = \begin{bmatrix} e_\xi \\ \dot{e}_\xi \end{bmatrix} = \begin{bmatrix} \xi_d - \xi \\ \dot{\xi}_d - \dot{\xi} \end{bmatrix} \tag{8}$$

$$E_\eta = \begin{bmatrix} e_\eta \\ \dot{e}_\eta \end{bmatrix} = \begin{bmatrix} \eta_d - \eta \\ \dot{\eta}_d - \dot{\eta} \end{bmatrix} \tag{9}$$

The objective of trajectory tracking control is to design the control input u and τ such that the tracking errors E_ξ and E_η converge to zero asymptotically. The six outputs $[x,\ y,\ z,\ \phi,\ \theta,\ \psi]^T$ are controlled by four inputs $[u,\ \tau_1,\ \tau_2,\ \tau_3]^T$ only. In order to deal with the underactuated part (Cartesian positions) of the system, three virtual control inputs are introduced with u, ϕ, and θ as follows

$$v = \begin{bmatrix} v_x \\ v_y \\ v_z \end{bmatrix} = \begin{bmatrix} (c\phi s\theta c\psi + s\phi s\psi)u \\ (c\phi s\theta s\psi - s\phi c\psi)u \\ c\phi c\theta u \end{bmatrix} \tag{10}$$

Here, the position $\xi(t)$ and yaw angle $\psi(t)$ are chosen as the states to be controlled. The desired position ξ_d and the desired yaw angle ψ_d are set by the guidance system, whereas the desired pitch and roll angles ϕ_d and θ_d are generated by the solution of the virtual control input v.

The total thrust u and $\phi_d(t)$, $\theta_d(t)$ can be obtained as [39]

$$\begin{cases} \phi_d = \sin^{-1}\left(\dfrac{v_x \sin\psi_d - v_y \cos\psi_d}{u}\right) \\ \theta_d = \tan^{-1}\left(\dfrac{v_x \cos\psi_d + v_y \sin\psi_d}{v_z}\right) \\ u = \sqrt{v_x^2 + v_y^2 + v_z^2} \end{cases} \tag{11}$$

Remark 2. The reference trajectory $\xi_d(t)$ and $\psi_d(t)$ are designed such that $\xi_d^{(i)}(t) \in L_\infty$, $\psi_d^{(j)}(t) \in L_\infty$ for $i = 1, 2$ and $j = 1,\ 2,\ 3$ to avoid the sudden change of the quadrotor's dynamic states, where the superscript (i) or (j) represents the i-th or j-th order time derivative of the variable.

Controller design

Outer-loop position tracking controller based on APD-SMC

This section presents the hierarchical model-free tracking controller design. In order to achieve robust position tracking performance without the requirement for the quadrotor dynamic model, APD-SMC law is proposed in the outer loop to control the position of the quadrotor UAV. A continuous robust RISE feedback method is employed in the inner loop for attitude tracking control to compensate for the unknown disturbances. The block diagram of the overall control system is shown in Figure 2.

The objective of this section is to design the virtual control input v to guarantee the globally asymptotically stability of the outer loop system and ensure the position tracking errors converge to zero. From equation (4), the outer loop subsystem can be described as

$$m\ddot{\xi} = -K_\xi\dot{\xi} + v - mge - d_\xi \tag{12}$$

The position tracking error e_ξ and its derivatives $\dot{e}_\xi$ and $\ddot{e}_\xi$ are defined as follows

$$e_\xi = \xi_d - \xi \tag{13}$$

$$\dot{e}_\xi = \dot{\xi}_d - \dot{\xi} \tag{14}$$

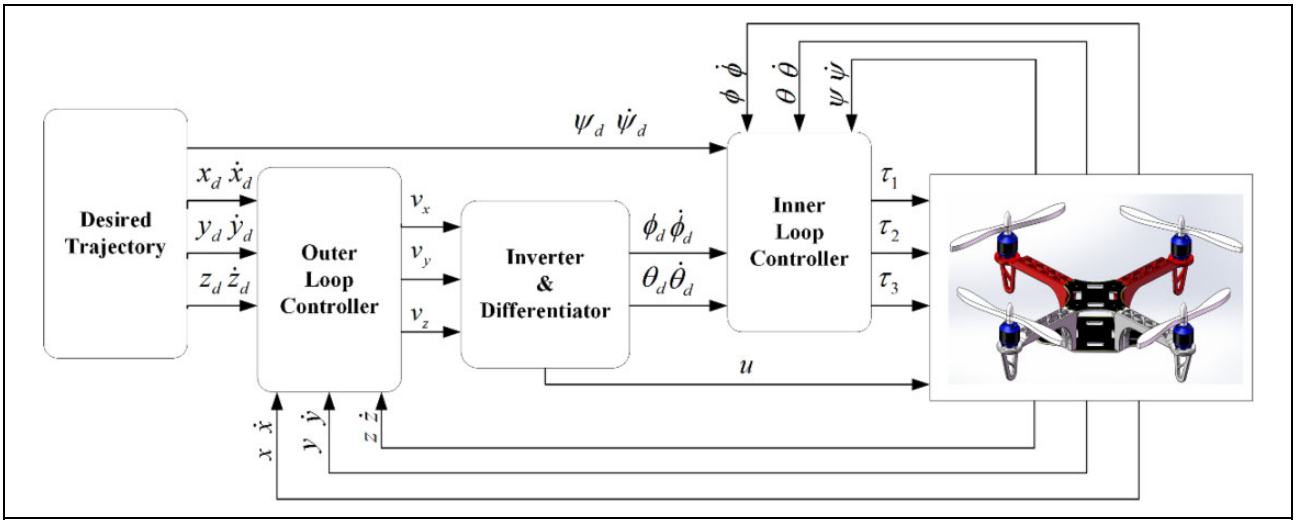

Figure 2. Block diagram of the overall control system.

$$\ddot{e}_\xi = \ddot{\xi}_d - \ddot{\xi} \tag{15}$$

Substituting equations (13) to (15) into equation (12), the dynamic model can be rewritten in the form of tracking errors as

$$m\ddot{e}_\xi + K_\xi \dot{e}_\xi = p - v \tag{16}$$

where $p = [p_1, p_2, p_3]^T = m\ddot{\xi}_d + K_\xi \dot{\xi}_d + mge + d_\xi$ represents the desired control input. On the basis of assumption 1 and remark 2, the desired control input p is bounded

$$\begin{aligned} p_1 &\le ||m\ddot{x}_d + K_{\xi 1}\dot{x}_d + d_{\xi 1}|| \le ||m\ddot{x}_d + K_{\xi 1}\dot{x}_d|| + ||d_{\xi 1}|| = P_{b1} \\ p_2 &\le ||m\ddot{y}_d + K_{\xi 2}\dot{y}_d + d_{\xi 2}|| \le ||m\ddot{y}_d + K_{\xi 2}\dot{y}_d|| + ||d_{\xi 2}|| = P_{b2} \\ p_3 &\le ||m\ddot{z}_d + K_{\xi 3}\dot{z}_d + d_{\xi 3} + mg|| \le ||m\ddot{z}_d + K_{\xi 3}\dot{z}_d + mg|| + ||d_{\xi 3}|| = P_{b3} \end{aligned} \tag{17}$$

where $||\cdot||$ represents the Euclidean norm and P_{bi} is the boundary of p_i $(i = 1, 2, 3)$.

From equation (16), it can be proved that the tracking errors could converge to zero if $v = p - K_\xi e_\xi - m\ddot{e}_\xi$. However, the information of p can be got only if the translational motion dynamic model is known accurately, which is not available in practice. Aiming at this problem, the APD-SMC law for the position tracking control of the quadrotor is proposed as

$$v = K_p e_\xi + K_d \dot{e}_\xi + \hat{P}_b + Hsign(\dot{e}_\xi + \mu e_\xi) \tag{18}$$

where $\hat{P}_b = [\hat{P}_{b1}, \hat{P}_{b2}, \hat{P}_{b3}]^T$ is the estimation of P_b; $sign(\cdot)$ is the sign function; $K_p = \text{diag}(K_{p1}, K_{p2}, K_{p3})$ and $K_d = \text{diag}(K_{d1}, K_{d2}, K_{d3})$ are the proportional and derivative control gain matrices of PD control; and $H = \text{diag}(h_1, h_2, h_3)$ is the SMC control gain matrix. The adaptive updating law $\dot{\hat{P}}_b$ is designed as

$$\dot{\hat{P}}_b = (\dot{e}_\xi + \mu e_\xi) \tag{19}$$

where $\mu = \text{diag}(\mu_1, \mu_2, \mu_3)$ is the sliding surface slope constant matrix.

Remark 3. The control law proposed in equation (18) is a combination of linear PD control and nonlinear SMC. The PD control which replaces the equivalent control part of the standard SMC is used to stabilize the nominal model, while the SMC and adaptive control are used to compensate for the unknown terms and improve robustness.

Remark 4. It can be seen that the APD-SMC law in equation (18) is only related to e_ξ and $\dot{e}_\xi$. Therefore, the control law is model-free and easy to be implemented in practical applications. Compared with the PD-SMC law in Ouyang et al.,[30] the proposed APD-SMC utilizes the adaptive method to estimate P_b. By introducing the estimation, the APD-SMC could achieve null steady-state error tracking capability with reasonable control gains such that the need for large control gains of PD-SMC to compensate for the unknown term p is avoided.

Lemma 1. A matrix L is defined as follows

$$L = \begin{bmatrix} K_p & m\mu \\ (m\mu)^T & mI_{3\times 3} \end{bmatrix} \tag{20}$$

If $\lambda_m(K_p) > \lambda_M(m\mu^2)$, then $L \succ 0$. That is, L is positive definite. $\lambda_m(\cdot)$ and $\lambda_M(\cdot)$ represent the smallest and largest eigenvalues of a positive-definite matrix, respectively.

Proof. As K_p, $m\mu$, and $m\mu^2$ are diagonal matrices, therefore, the matrix L is a symmetric matrix

$$L = \begin{bmatrix} K_p & m\mu \\ m\mu & mI_{3\times 3} \end{bmatrix} \tag{21}$$

If $\lambda_m(K_p) > \lambda_M(m\mu^2)$, then,

$$K_p - m\mu^2 \succ 0 \tag{22}$$

$$(mI_{3\times3})^{-1} - \mu^2 K_p^{-1} \succ 0 \tag{23}$$

As $mI_{3\times3} \succ 0$, therefore

$$mI_{3\times3} - m\mu^2 K_p^{-1} mI_{3\times3} \succ 0 \tag{24}$$

The Schur complement[40] of K_p in L is

$$S = mI_{3\times3} - (m\mu)^T K_p^{-1}(m\mu) \succ 0 \tag{25}$$

Thus, $K_p \succ 0$, $S \succ 0$.
Finally, $L \succ 0$.

Theorem 1. Considering the outer loop subsystem in equation (12) with the proposed APD-SMC law in equation (18) and the adaption law in equation (19), the controlled system is globally asymptotically stable and the tracking error E_ξ in equation (8) could converge to zero if the control gains and parameters satisfy the conditions as follows

$$\begin{cases} \mu_i > 0 \\ h_i \geq P_{bi} - p_i > 0 \\ \lambda_m(K_\xi + K_d) > \lambda_M(m\mu) \\ \lambda_m(K_p) > \lambda_M(m\mu^2) \end{cases} \tag{26}$$

Remark 5. For most translational robotic systems, their dynamics can be described as $M\ddot{X} + K_\xi \dot{X} + d = v$. M, K_ξ, and d are mass matrix, damping matrix, and disturbance, respectively.[30] If the assumption that M, K_ξ, and d are all bounded holds and their desired trajectory X_d satisfy that $\dot{X}_d \in L_\infty$, $\ddot{X}_d \in L_\infty$, then the robotic system could satisfy the condition (26) by choosing proper control gains.

For the quadrotor outer loop system described in equation (12), it is reasonable to assume that the mass m, aerodynamic damping matrix K_ξ, and the disturbance d_ξ are bounded. By combining with remark 2, it is easy to get that p_i $(i = 1, 2, 3)$ is bounded (17). Finally according to remark 5, the conditions in equation (26) can be easily satisfied by choosing proper control gains μ_i, h_i, $(i = 1, 2, 3)$, K_d, and K_p.

Proof. Substituting equation (18) into equation (16), the dynamic model can be rewritten as

$$m\ddot{e}_\xi + (K_\xi + K_d)\dot{e}_\xi + K_p e_\xi = p - \hat{P}_b - Hsign(\dot{e}_\xi + \mu e_\xi) \tag{27}$$

A positive Lyapunov function is defined as follows

$$V(e_\xi, \dot{e}_\xi) = \frac{1}{2}(e_\xi{}^T, \dot{e}_\xi{}^T) L \begin{pmatrix} e_\xi \\ \dot{e}_\xi \end{pmatrix} + \frac{1}{2} e_\xi{}^T \mu (K_\xi + K_d) e_\xi + \tilde{P}_b^T \tilde{P}_b \tag{28}$$

where $\tilde{P}_b = P_b - \hat{P}_b$. The time derivative of the Lyapunov function is

$$\begin{aligned} \dot{V}(e_\xi, \dot{e}_\xi) = & -e_\xi{}^T \mu K_p e_\xi - \dot{e}_\xi{}^T (K_\xi + K_d - m\mu)\dot{e}_\xi \\ & + (\dot{e}_\xi{}^T + e_\xi{}^T \mu)(p - \hat{P}_b - Hsign(\dot{e}_\xi + \mu e_\xi)) - \dot{\hat{P}}_b^T \tilde{P}_b \end{aligned} \tag{29}$$

Substituting equation (19) into equation (29), one can get

$$\begin{aligned} \dot{V}(e_\xi, \dot{e}_\xi) = & -e_\xi{}^T \mu K_p e_\xi - \dot{e}_\xi{}^T (K_\xi + K_d - m\mu)\dot{e}_\xi \\ & + (\dot{e}_\xi{}^T + e_\xi{}^T \mu)(p - P_b - Hsign(\dot{e}_\xi + \mu e_\xi)) \end{aligned} \tag{30}$$

If $\mu_i > 0$ and $\lambda_m(K_\xi + K_d) > \lambda_M(m\mu)$, then

$$-e_\xi^T \mu K_p e_\xi < 0 \tag{31}$$

and

$$-\dot{e}_\xi^T (K_\xi + K_d - m\mu)\dot{e}_\xi^T < 0 \tag{32}$$

If $h_i \geq P_{bi} - p_i > 0$, then

$$\begin{aligned} & (\dot{e}_\xi{}^T + e_\xi{}^T \mu) Hsign(\dot{e}_\xi + \mu e_\xi) \\ & > ||(\dot{e}_\xi{}^T + e_\xi{}^T \mu)||_1 ||(P_b - p)||_1 > (\dot{e}_\xi{}^T + e_\xi{}^T \mu)(p - P_b) \end{aligned} \tag{33}$$

where $||\cdot||_1$ denote the 1-norm.

Thus,

$$(\dot{e}_\xi{}^T + e_\xi{}^T \mu)(p - P_b - Hsign(\dot{e}_\xi + \mu e_\xi)) < 0 \tag{34}$$

Therefore,

$$\dot{V}(e_\xi, \dot{e}_\xi) < 0 \tag{35}$$

The Lyapunov function $V(e_\xi, \dot{e}_\xi)$ is positive and its time derivative $\dot{V}(e_\xi, \dot{e}_\xi)$ is negative. According to the Lyapunov method, the outer loop subsystem is globally asymptotically stable with the APD-SMC in equation (18) and the tracking error E_ξ could converge to zero.

Remark 6. The $sign(\cdot)$ function in APD-SMC law could cause the chattering. In order to eliminate chattering, a saturation function $\tanh(\cdot)$ is used to replace the discontinuous $sign(\cdot)$ function. Then, the control law in equation (18) is modified into

$$v = K_p e_\xi + K_d \dot{e}_\xi + \hat{P}_b + H \tanh(\dot{e}_\xi + \mu e_\xi) \tag{36}$$

Inner-loop attitude tracking controller based on RISE

The objective of this section is to design the proper control inputs τ_i $(i = 1, 2, 3)$ to guarantee the locally exponentially stability of the inner loop system and ensure the tracking error E_η in equation (9) converge to zero. A simplified inner-loop dynamic model is used to facilitate the RISE feedback controller design. The simplified dynamic model is given as follows[41,42]

$$J\ddot{\eta} = \tau - K_\eta \dot{\eta} + d_\eta \tag{37}$$

where $K_\eta = \text{diag}(K_{\eta1}, K_{\eta2}, K_{\eta3})$ is the rotational aerodynamic damping matrix. The aerodynamic damping coefficients $K_{\eta1}$, $K_{\eta2}$, and $K_{\eta3}$ are positive constants.

The attitude tracking error $e_{\eta1}$ and its filtered error signals $e_{\eta2}$ and $e_{\eta3}$ are defined as follows

$$e_{\eta1} = \eta_d - \eta \tag{38}$$

$$e_{\eta2} = \dot{e}_{\eta1} + \lambda e_{\eta1} \tag{39}$$

$$e_{\eta3} = \dot{e}_{\eta2} + \alpha e_{\eta2} \tag{40}$$

where $\lambda = \text{diag}(\lambda_1, \lambda_2, \lambda_3)$ and $\alpha = \text{diag}(\alpha_1, \alpha_2, \alpha_3)$ are positive-definite gain matrices, and $\lambda_i > \frac{1}{2}, \alpha_i > \frac{1}{2}, i = 1, 2, 3$.

The auxiliary functions $N(t)$, $N_d(t)$, and $\tilde{N}(t)$ are defined as follows

$$N(t) = J(\ddot{\eta}_d + \lambda\ddot{e}_{\eta1} + \alpha\dot{e}_{\eta2}) + K_\eta\ddot{\eta} - \dot{d}_\eta + e_{\eta2} \tag{41}$$

$$N_d(t) = J\ddot{\eta}_d + K_\eta\ddot{\eta}_d - \dot{d}_\eta \tag{42}$$

$$\tilde{N}(t) = N(t) - N_d(t) \tag{43}$$

According to remark 2, $N(t)$ is continuous differentiable. $N_d(t)$ and $\dot{N}_d(t)$ are bounded.[32] It is easy to prove that $\tilde{N}(t)$ is also bounded as

$$||\tilde{N}(t)|| \leq \rho||\Gamma|| \tag{44}$$

where the error vector Γ is defined as $\Gamma = [e_{\eta1}, e_{\eta2}, e_{\eta3}]^T$. ρ is a positive constant.

The RISE feedback control law is chosen as

$$\tau = (K_s + I_{3\times3})\left(e_{\eta2}(t) - e_{\eta2}(0) + \int_0^t \alpha e_{\eta2}(\tau)\ d\tau\right) + \int_0^t \beta sign(e_{\eta2}(\tau))d\tau \tag{45}$$

where $K_s = \text{diag}(K_{s1}, K_{s2}, K_{s3})$, $\beta = \text{diag}(\beta_1, \beta_2, \beta_3)$ are positive-definite control gain matrices. $I_{3\times3}$ is the identity matrix.

Remark 7. The inner loop control input designed in equation (45) is only related to the filtered tracking error $e_{\eta2}$ and no dynamic model is needed. Therefore, the control law in equation (45) is model-free. Moreover, $\int_0^t \beta sign(e_{\eta2}(\tau))d\tau$, the integrating of function $sign(e_{\eta2}(\tau))$ makes the proposed control law become continuous and then the chattering problem is avoided. The model-free continuous RISE control law is physically realizable.

Next, the locally exponentially stable of the inner loop system is proven while a lemma is stated first.

Lemma 2. An auxiliary function $Q(t)$ is defined as follows

$$Q(t) = {e_{\eta3}}^T(N_d(t) - \beta sign(e_{\eta2})) \tag{46}$$

If the control gain matrix $\beta = \text{diag}(\beta_1, \beta_2, \beta_3)$ satisfies

$$\beta_i > ||N_d(t)||_\infty + \frac{1}{\alpha_i}||\dot{N}_d(t)||_\infty \tag{47}$$

then,

$$\int_0^t Q(\tau)d\tau \leq \varpi \tag{48}$$

where ϖ is a positive constant defined as

$$\varpi = ||\beta e_{\eta2}(0)||_1 - e_{\eta2}^T(0)N_d(0) \tag{49}$$

and $||\cdot||_\infty$ denotes the infinite-norm.

Proof. Applying equation (40), equation (46) can be rewritten as

$$\begin{aligned}
\int_0^t Q(\tau)d\tau &= \int_0^t e_{\eta2}^T(\tau)\alpha(N_d(\tau) - \beta sign(e_{\eta2}(\tau)))d\tau + \int_0^t \frac{de_{\eta2}^T(\tau)}{d\tau}N_d(\tau)d\tau - \int_0^t \frac{de_{\eta2}^T(\tau)}{d\tau}\beta sign(e_{\eta2}))d\tau \\
&= \int_0^t e_{\eta2}^T(\tau)\alpha(N_d(\tau) - \beta sign(e_{\eta2}(\tau)))d\tau + \left(e_{\eta2}^T(\tau)N_d(\tau)\right)\Big|_0^t - \int_0^t e_{\eta2}^T\frac{d(N_d(\tau))}{d\tau}d\tau - \sum_{i=1}^3 \beta_i|e_{\eta2i}(\tau)|\Big|_0^t \\
&= \int_0^t e_{\eta2}^T(\tau)\alpha\left(N_d(\tau) - \alpha^{-1}\frac{d(N_d(\tau))}{d\tau} - \beta sign(e_{\eta2}(\tau))\right)d\tau + e_{\eta2}^T(t)N_d(t) - e_{\eta2}^T(0)N_d(0) \\
&\quad + \sum_{i=1}^3 \beta_i|e_{\eta2i}(0)| - \sum_{i=1}^3 \beta_i|e_{\eta2i}(t)|
\end{aligned} \tag{50}$$

Then, one of its upper bound is obtained as follows

$$\int_0^t Q(\tau)d\tau \le \int_0^t \left|e_{\eta 2}^T(\tau)\alpha\right|\left(|N_d(\tau)| + \alpha^{-1}\left|\frac{d(N_d(\tau))}{d\tau}\right| - \beta\right)d\tau + \sum_{i=1}^{3}|e_{\eta 2i}(t)|(N_{di}(t)-\beta_i) + \sum_{i=1}^{3}\beta_i|e_{\eta 2i}(0)| - e_{\eta 2}^T(0)N_d(0)$$
$$\le \sum_{i=1}^{3}\beta_i|e_{\eta 2i}(0)| - e_{\eta 2}^T(0)N_d(0) \tag{51}$$

If β_i $(i = 1, 2, 3)$ is chosen according to equation (47), then

$$\int_0^t Q(\tau)d\tau \le \sum_{i=1}^{3}\beta_i|e_{\eta 2i}(0)| - e_{\eta 2}^T(0)N_d(0) = ||\beta e_{\eta 2}(0)||_1 - e_{\eta 2}^T(0)N_d(0) \tag{52}$$

Therefore,

$$\int_0^t Q(\tau)d\tau \le \varpi \tag{53}$$

Theorem 2. Given the attitude control system in equation (37) and provided that the control gains β_i $(i = 1, 2, 3)$ satisfy the conditions in equation (47), the attitude controller in equation (45) could guarantee the locally exponentially stability of the controlled system and the convergence of the tracking error E_η in equation (9).

Proof. Define a Lyapunov function as follows

$$V(\Gamma, t) = \frac{1}{2}e_{\eta 1}^T e_{\eta 1} + \frac{1}{2}e_{\eta 2}^T e_{\eta 2} + \frac{1}{2}e_{\eta 3}{}^T J e_{\eta 3} + \sigma(t) \tag{54}$$

where $\sigma(t)$ is defined as

$$\sigma(t) = \varpi - \int_0^t Q(\tau)d\tau \tag{55}$$

It can be seen that equation (46) in lemma 2 ensures that $\sigma(t) > 0$. Thus, the Lyapunov function in equation (54) is positive.

The time differentiation of $V(\Gamma, t)$ is

$$\dot{V}(\Gamma, t) = e_{\eta 1}^T\dot{e}_{\eta 1} + e_{\eta 2}^T\dot{e}_{\eta 2} + e_{\eta 3}{}^T J\dot{e}_{\eta 3} + \dot{\sigma}(t) \tag{56}$$

Substituting equations (41) to (43) and equation (45) into equation (37), the closed-loop subsystem of $e_{\eta 3}$ can be obtained

$$J\dot{e}_{\eta 3} = -e_{\eta 2} - (K_s + I_{3\times 3})e_{\eta 3} - \beta\,\mathrm{sgn}(e_{\eta 2}) + \tilde{N}(t) + N_d(t) \tag{57}$$

Substituting equations (38) to (40) and equation (57) into equation (56)

$$\dot{V}(\Gamma, t) = e_{\eta 1}^T e_{\eta 2} - e_{\eta 1}^T\lambda e_{\eta 1} - e_{\eta 2}^T\alpha e_{\eta 2} - e_{\eta 3}{}^T K_s e_{\eta 3} - e_{\eta 3}{}^T e_{\eta 3} + e_{\eta 3}{}^T\tilde{N}(t) + [e_{\eta 3}{}^T\left(N_d(t) - \beta sign(e_{\eta 2})\right) - Q(t)] \tag{58}$$

Equation (46) in lemma 2 ensures the term $[e_{\eta 3}{}^T\left(N_d(t) - \beta sign(e_{\eta 2})\right) - Q(t)]$ in equation (58) cancel out. With equation (44) and the fact that $e_{\eta 1}^T e_{\eta 2} \le \frac{1}{2}(e_{\eta 1}^T e_{\eta 1} + e_{\eta 2}^T e_{\eta 2})$, an upper bound on equation (58) is obtained as follows

$$\dot{V}(\Gamma, t) \le -\delta||\Gamma||^2 + ||e_{\eta 3}||\rho||\Gamma|| - e_{\eta 3}{}^T K_s e_{\eta 3} \le -\left(\delta - \frac{\rho^2}{4\vartheta}\right)||\Gamma||^2 \tag{59}$$

where the positive constants δ and ϑ are defined as $\delta = \min\{1,\ \alpha_i - \frac{1}{2},\ \lambda_i - \frac{1}{2}\}$, $\vartheta = \min\{K_{si}\}$ $(i = 1, 2, 3)$.

Thus,

$$\dot{V}(\Gamma, t) \le -\ell||\Gamma||^2 \ \text{ for } \vartheta > \frac{\rho^2}{4\delta} \tag{60}$$

where ℓ is a positive constant. Based on the Lyapunov method, the inner loop is locally exponentially stable and the attitude tracking error E_η in equation (9) converges to zero.

Remark 8. The attitude control law in equation (45) requires not only the desired attitude angle η_d but also the desired angular velocity $\dot{\eta}_d$. The desired pitch and roll angles, ϕ_d and θ_d, are generated by the solutions of the virtual control inputs v_i $(i = 1, 2, 3)$. Taking the derivative with respect to the desired attitude angles may cause infinity problem. In order to solve this problem, a tracking differentiator[43] is used.

The tracking differentiator is designed as follows

$$\begin{cases} \dot{x}_{1\Phi} = x_{2\Phi} \\ \dot{x}_{2\Phi} = -r_\Phi sign\left(x_{1\Phi} - \Phi(t) + \dfrac{x_{2\Phi}|x_{2\Phi}|}{2r_\Phi}\right) \end{cases} \tag{61}$$

where $\Phi(t)$ is the input signal needed to be differentiated. $x_{1\Phi}$ tracks $\Phi(t)$ and $x_{2\Phi}$ tracks $\dot{(}t)$. r_Φ is a positive constant which determines the tracking speed.

Let $\phi_d(t)$ or $\theta_d(t)$ be the input of the tracking differentiator, respectively, that is, $\Phi(t) = \phi_d(t)$ or $\Phi(t) = \theta_d(t)$. Then, $\dot{\phi}_d(t)$ and $\dot{\theta}_d(t)$ can be obtained

$$\dot{\phi}_d(t) \approx \int_0^t -r_\Phi sign\left(x_{1\Phi} - \phi_d(\tau) + \frac{x_{2\Phi}|x_{2\Phi}|}{2r_\Phi}\right)d\tau \quad (62)$$

$$\dot{\theta}_d(t) \approx \int_0^t -r_\Phi sign\left(x_{1\Phi} - \theta_d(\tau) + \frac{x_{2\Phi}|x_{2\Phi}|}{2r_\Phi}\right)d\tau \quad (63)$$

Remark 9. It can be seen in equations (62) and (63) that, $\int_0^t -r_\Phi sign\left(x_{1\Phi} - \phi_d(\tau) + \frac{x_{2\Phi}|x_{2\Phi}|}{2r_\Phi}\right)d\tau$, $\int_0^t -r_\Phi sign\left(x_{1\Phi} - \theta_d(\tau) + \frac{x_{2\Phi}|x_{2\Phi}|}{2r_\Phi}\right)d\tau$, the integrating of $sign(x_{1\Phi} - \phi_d(\tau) + \frac{x_{2\Phi}|x_{2\Phi}|}{2r_\Phi})$ and $sign\left(x_{1\Phi} - \theta_d(\tau) + \frac{x_{2\Phi}|x_{2\Phi}|}{2r_\Phi}\right)$ make the $\dot{\phi}_d(t)$ and $\dot{\theta}_d(t)$ become continuous and the chattering problem caused by the $sign(\cdot)$ function is avoided.

Simulation results

Extensive simulation experiments have been done to demonstrate the effectiveness and robustness of the proposed control strategy for trajectory tracking of a quadrotor. The quadrotor model parameters and their values are listed in Table 1, which are chosen from the test used in the study of Khatoon et al..[37] The simulation experiments compare the tracking performances of the proposed control strategy with those achieved by the PD+PD, PID+PID, MFTSMC,[18] adaptive[19] and PD-SMC+RISE controllers. The control gains of these controllers which are adjusted with trial and error are listed in Table 2. All the simulation experiments are conducted in Matlab R2016a on a PC with Intel (R) Core I7-4790 @ 3.6 GHz CPU, 8 GB RAM, and 1000 GB solid state disk drive.

Remark 10. PD+PD, PID+PID, and PD-SMC+RISE mean that the outer loop controllers of these control scheme are PD controller, PID controller, and PD-SMC, respectively, and the inner loop controllers are PD controller, PID controller, and RISE controller, respectively.

Case 1: Chattering eliminating

In this section, the trajectory tracking performances of the APD-SMC using $sign(\cdot)$ function (18) and that using $\tanh(\cdot)$ function (36) are given.

Table 2. Control gains.

Controllers	Outer loop gains	Inner loop gains
PD+PD	$K_p = \text{diag}(30, 30, 50)$	$K_p = \text{diag}(15, 15, 20)$
	$K_d = \text{diag}(10, 5, 30)$	$K_d = \text{diag}(10, 10, 10)$
PID+PID	$K_p = \text{diag}(20, 20, 30)$	$K_p = \text{diag}(50, 50, 50)$
	$K_i = \text{diag}(10, 10, 10)$	$K_i = \text{diag}(20, 20, 20)$
	$K_d = \text{diag}(5, 5, 10)$	$K_d = \text{diag}(10, 10, 10)$
Adaptive	$K_o = \text{diag}(8, 5, 5)$	$K_i = \text{diag}(5, 5, 10)$
	$\lambda = \text{diag}(5, 2, 5)$	$\lambda = \text{diag}(5, 5, 5)$
MFTSMC	$E = \text{diag}(0.3, 2.5, 0.8, 0.1, 0.1, 0.1)$, $p = 1.2$,	
	$\lambda = \text{diag}(0.1, 0.1, 0.4, 0.6, 0.5, 0.5)$, $q = 0.8$,	
	$\beta = \text{diag}(0.5, 0.2, 2, 0.5, 0.5, 0.1)$,	
	$\alpha = \text{diag}(40, 100, 60, 100, 40, 150)$	
PD-SMC+RISE	$K_p = \text{diag}(30, 20, 20)$	$\alpha = \text{diag}(50, 50, 20)$
	$K_d = \text{diag}(10, 10, 10)$	$\lambda = \text{diag}(50, 50, 15)$
	$H = \text{diag}(30, 20, 30)$	$K_s = \text{diag}(10, 5, 10)$
	$\mu = \text{diag}(10, 10, 10)$	$\beta = \text{diag}(4, 5, 10)$
APD-SMC+RISE	$K_p = \text{diag}(17, 15, 15)$	$\alpha = \text{diag}(50, 50, 20)$
	$K_d = \text{diag}(10, 7, 10)$	$\lambda = \text{diag}(50, 50, 15)$
	$H = \text{diag}(5, 5, 5)$	$K_s = \text{diag}(10, 5, 10)$
	$\mu = \text{diag}(10, 10, 5)$	$\beta = \text{diag}(4, 5, 10)$

PD: proportional derivative; MFTSMC: model-free terminal sliding mode controller; SMC: sliding mode control; RISE: robust integral of the signum of the error; APD: adaptive proportional derivative.

The desired trajectory is given as

$$\begin{cases} x_d = 0 \ (m) \\ y_d = 0 \ (m) \\ z_d = 5\sin(2\pi/60)t \ (m) \end{cases} \quad (t < 15s)$$

$$\begin{cases} x_d = 0 \ (m) \\ y_d = 0 \ (m) \\ z_d = 5 \ (m) \end{cases} \quad (15\,\text{s} \le t < 20\,\text{s}) \quad (64)$$

$$\begin{cases} x_d = 1 - \cos\left(0.25(t-20)\right) \ (\text{m}) \\ y_d = \sin\left(0.5(t-20)\right) \ (\text{m}) \\ z_d = 5 \ (m) \end{cases} \quad (t \ge 20\,\text{s})$$

The initial position and attitude of the quadrotor are set as $[x(0), y(0), z(0)] = [0 \ \ 0 \ \ 0](\text{m})$ and $[\phi(0), \theta(0), \psi(0)] = [0 \ \ 0 \ \ 0](\text{rad})$, respectively. The control gains of the APD-SMC law using $sign(\cdot)$ function (18) are $K_p = \text{diag}(15, 15, 15)$, $K_d = \text{diag}(8, 10, 5)$, $H = \text{diag}(5, 5, 5)$, $\mu = \text{diag}(10, 10, 5)$. The control gains of the APD-SMC

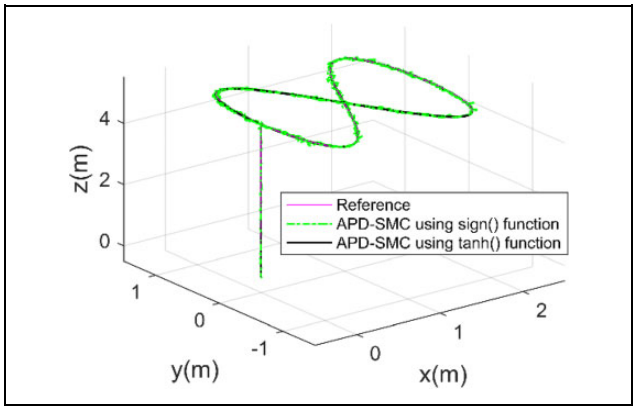

Figure 3. Trajectories in 3-D space. 3-D: three-dimensional.

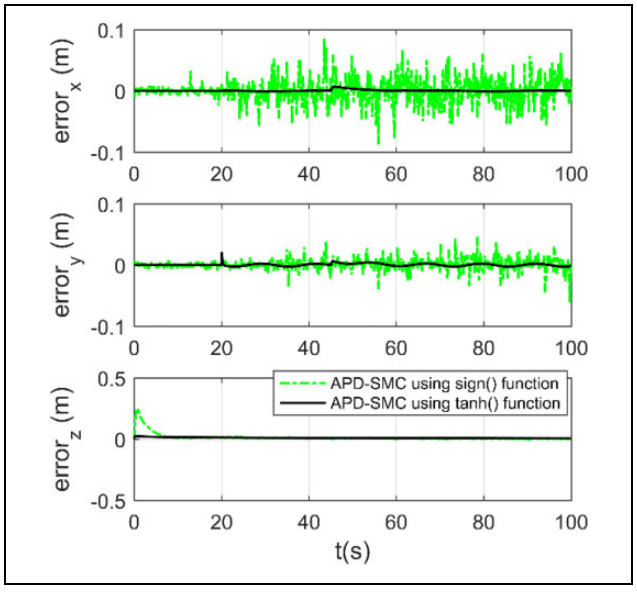

Figure 4. Position tracking error.

law using $\tanh(\cdot)$ (36) are listed in Table 2. The external disturbances are introduced as

$$d_{\xi i} = 0.5(\mathrm{N})\ \text{at};\ t \geq 45\,\mathrm{s}$$

$$d_{\eta i} = 0.6\sin(t+20) + 0.6\cos(t+20)\ \ (\mathrm{N\,m}).$$

The trajectory tracking results are shown in Figure 3. Position tracking errors are depicted in Figure 4. The virtual control inputs v_i $(i = 1, 2, 3)$ are depicted in Figure 4. As shown in Figures 3 and 4, both the APD-SMC using the $sign(\cdot)$ function (18) and that using the $\tanh(\cdot)$ function (36) can drive the quadrotor to track the desired trajectory in the presence of disturbances. However, the discontinuous $sign(\cdot)$ function induces serious chattering as shown in Figure 5. The undesirable control signals may cause damage and tear and wear in the quadrotor system and even lead to the system breakdown. In contrast, by replacing the discontinuous $sign(\cdot)$ function with the $\tanh(\cdot)$ function, the chattering can be eliminated and the continuous control

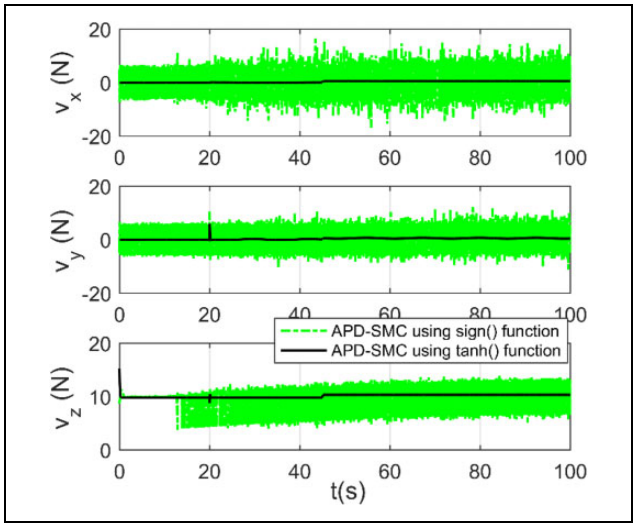

Figure 5. Virtual control inputs.

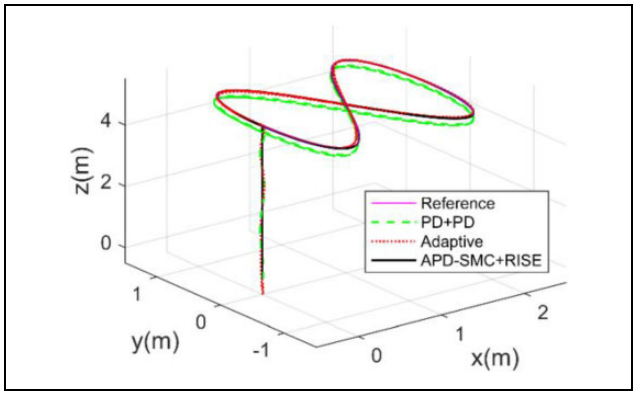

Figure 6. Reference trajectory and the tracking trajectories of different controllers in 3-D space. 3-D: three-dimensional.

signals make it easier to apply the APD-SMC law in equation (36) in practical applications.

Case 2: Comparison of trajectory tracking performances of different controllers

In this case, trajectory tracking performances of PD+PD controller, adaptive controller[19] and APD-SMC+RISE controller are given. The reference trajectory, quadrotor initial states, and external disturbances are the same with those in case 1.

The tracking performance of the proposed control strategy is compared with those achieved with PD+PD controller and adaptive controller. The reference trajectory and the tracking trajectories are shown in Figure 6. The position tracking errors along three axes in the earth-frame coordinates are shown in Figures 7 to 9.

As shown in Figures 6 to 9, it can be seen that the quadrotor cannot obtain the null steady-state error with the PD+PD controller. When the time-invariant persistent disturbances $d_{\xi i} = 0.5(\mathrm{N})$ are introduced at $t = 45\,\mathrm{s}$, the

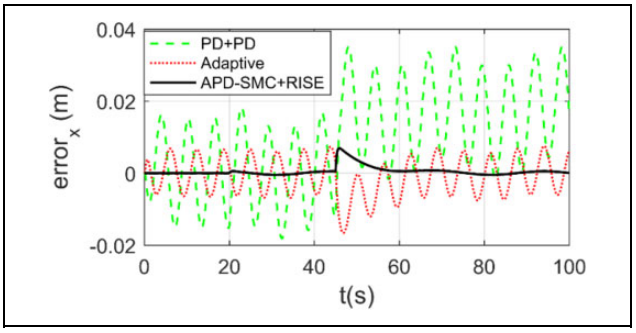

Figure 7. Position tracking error in *x*-axis.

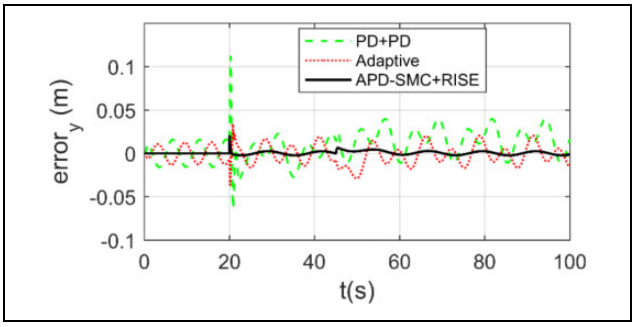

Figure 8. Position tracking error in *y*-axis.

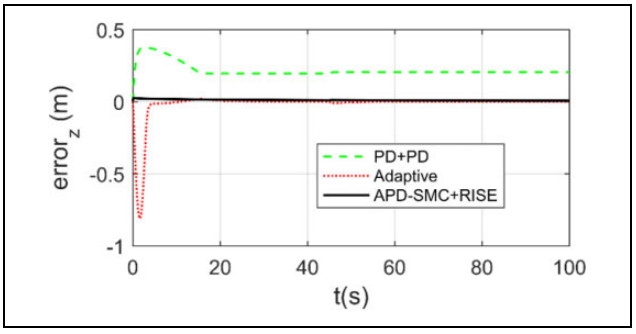

Figure 9. Position tracking error in *z*-axis.

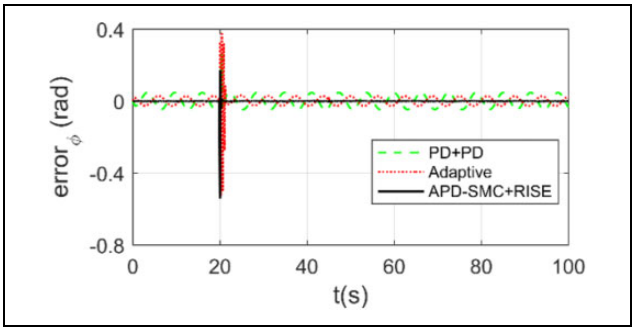

Figure 10. Roll angle tracking error.

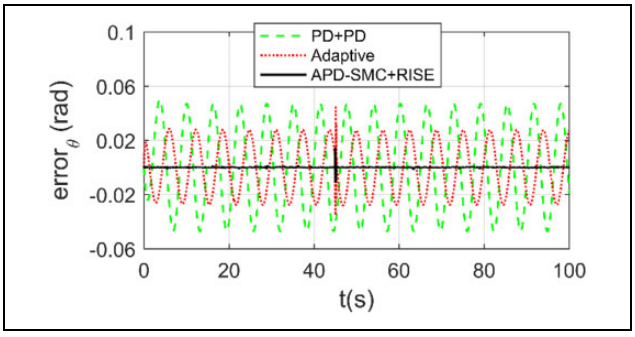

Figure 11. Pitch angle tracking error.

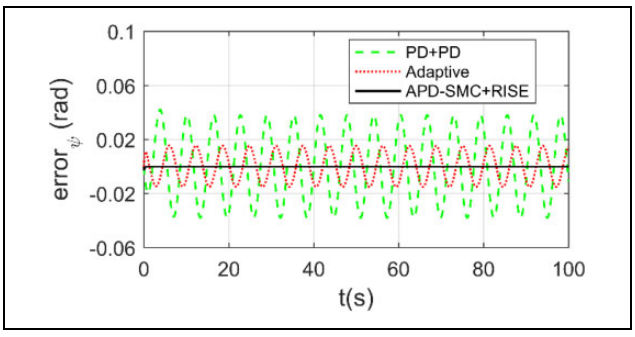

Figure 12. Yaw angle tracking error.

quadrotor with PD+PD controller leaves its predetermined trajectory and never reach the desired trajectory again. The reason is that the PD+PD controller lacks of the integral term for compensating the time-invariant persistent disturbances. As shown in Figure 9, PD+PD controller also cannot compensate for the steady-state error in *z*-axis induced by the gravity effect.

As is shown in Figure 9, significant error occurs at $t = 0 - 15\,\text{s}$ under the adaptive controller. The reason is that in the altitude control subsystem, the unknown term to be estimated is large and it takes time for the updating law to compensate for it. When the quadrotor is in hovering at $t > 15\,\text{s}$, the dynamic of the altitude control subsystem is slow such that the adaptive controller achieves good tracking performance. However, as shown in Figures 7 and 8, when the dynamics are fast time-varying, the performances of the adaptive controller along *x* and *y* axes are not as good as that of altitude tracking.

Compared with PD+PD controller and adaptive controller, the proposed APD-SMC+RISE controller could quickly response to the disturbance and drive the quadrotor UAV to the desired positions without steady-state error. In addition, as is shown in Figure 8, the aggressive upward desired linear speed command $\dot{y}_d$ at $t = 20\,\text{s}$ causes the significant tracking errors. Due to the strong robustness, the significant error under the APD-SMC+RISE controller is the smallest among the three ones.

The attitude controlling errors are shown in Figures 10 to 12. It can be seen that under the APD-SMC+RISE controller, the attitude trajectories are tracked with the highest accuracy. We can also see in Figures 10 and 11, because of the state changing, significant errors occur at $t = 20\,\text{s}$ and

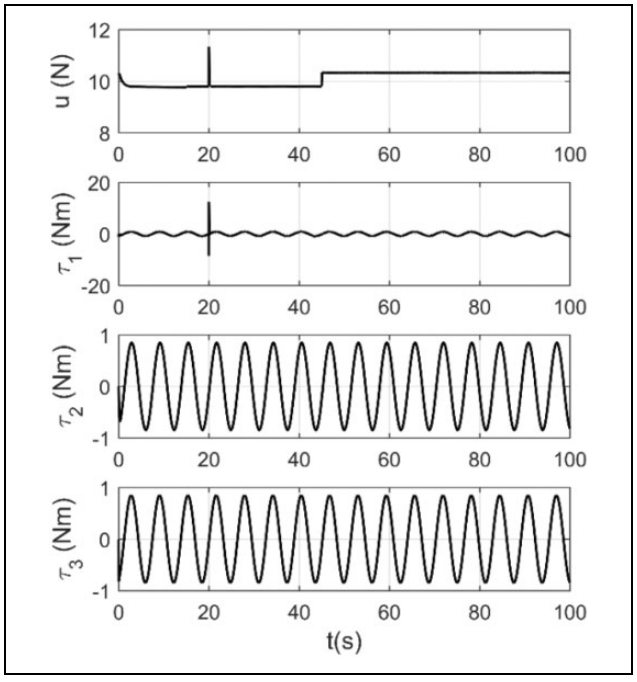

Figure 13. Control inputs.

$t = 45$ s, respectively. The APD-SMC+RISE controller could quickly response to the tracking errors and enables the attitude angles converge to their desired values in short time. The control inputs are depicted in Figure 13. It can be seen that the control inputs are continuous and the control signals are physically realizable.

Case 3: Trajectory tracking performances in case of wind gust

The trajectory tracking results of MFTSMC[18] and APD-SMC+RISE controller in the presence of wind gust are given. The desired trajectory is the same as that in case 1. The wind gust $d_{\xi i}$ is simulated by a Gaussian function with standard deviation of 0.1. The disturbances are given as

$$d_{\xi i} = 10\exp\left(-\frac{1}{2}\frac{(t-10)^2}{0.1^2}\right) + 10\exp\left(-\frac{1}{2}\frac{(t-60)^2}{0.1^2}\right)(\mathrm{N}),$$

$$d_{\eta i} = 2\sin(10t+50)(\mathrm{N\,m}).$$

Figure 14 shows the position tracking results of MFTSMC and APD-SMC+RISE in the presence of wind gust. Figures 15 to 17 present the position tracking errors.

It can be seen in Figures 15 to 17 that the two controllers could achieve satisfactory tracking performances. However, as is shown in Figure 17, it takes a long time for the MFTSMC to estimate the initial model of the altitude subsystem. In addition, when the wind gust is imposed on the quadrotor at $t = 10$ s, 60 s, there is a dramatic difference between the current model and the previous estimated model such that significant tracking error occurs under the MFTSMC. As is shown in Figures 18 and 19, the wind gust

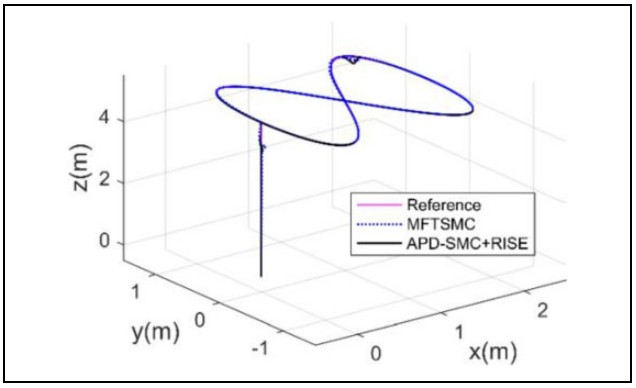

Figure 14. Tracking trajectories in case of wind gust in 3D space. 3-D: three-dimensional.

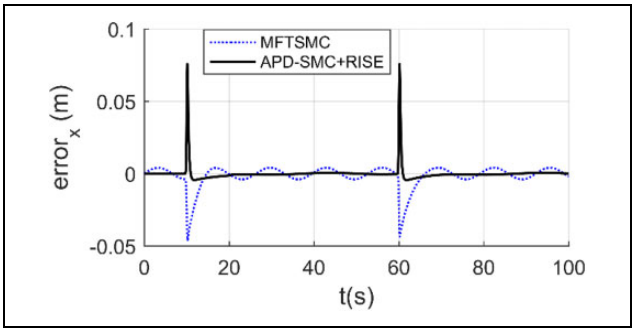

Figure 15. Position tracking error in *x*-axis.

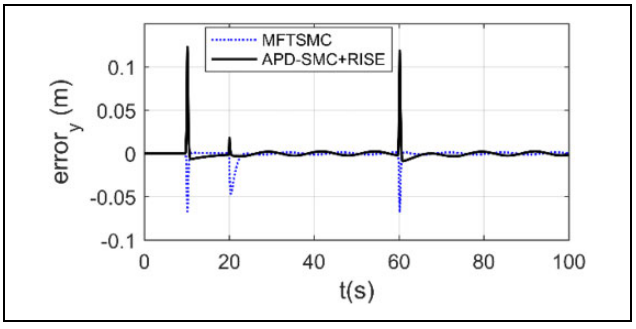

Figure 16. Position tracking error in *y*-axis.

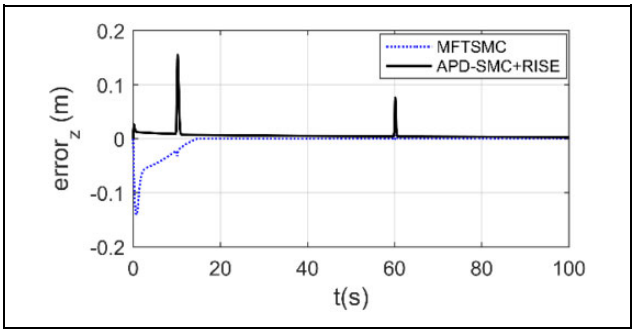

Figure 17. Position tracking error in *z*-axis.

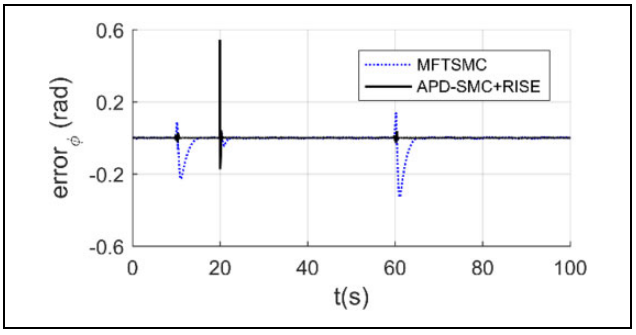

Figure 18. Roll angle tracking error.

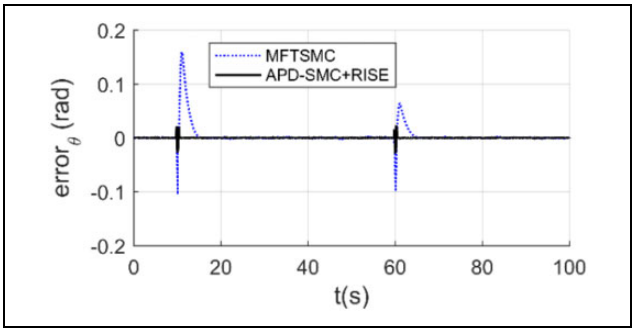

Figure 19. Pitch angle tracking error.

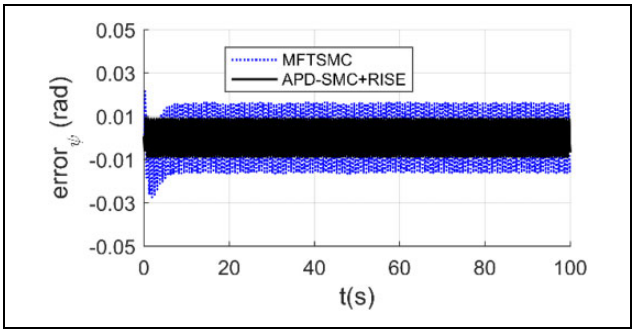

Figure 20. Yaw angle tracking error.

also has effect on the roll and pitch control subsystems such that significant tracking errors appear.

In contrast, as is shown in Figures 15 to 17, because there is no need to estimate the quadrotor dynamic model, the convergence time under the APD-SMC+RISE controller is much shorter than that of the MFTSMC. When the wind gust is introduced, the proposed controller could drive the quadrotor to the desired trajectory in short time. Attitude tracking errors are shown in Figures 18 to 20. It can be seen that the desired attitude trajectories are well tracked without significant errors under the APD-SMC+RISE controller.

Case 4: Space circle trajectory tracking in case of parametric variation

This section gives the tracking results of the PID+PID controller, PD-SMC+RISE controller, and APD-SMC+RISE

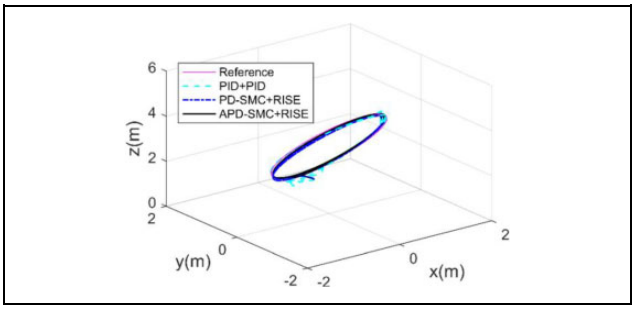

Figure 21. Space circle tracking performance of different controllers.

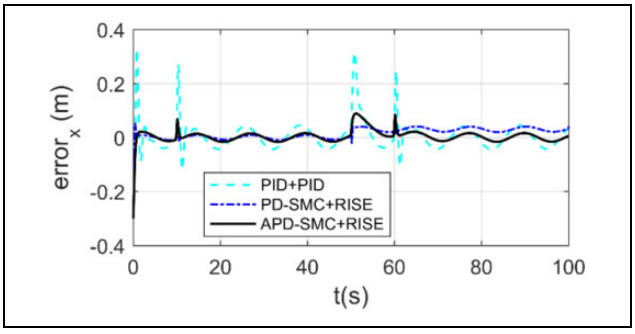

Figure 22. Position tracking error in *x*-axis.

controller in the presence of parametric variation. The desired trajectory is given as

$$\begin{cases} x_d = \sin(0.25t)\ \ (\mathrm{m}) \\ y_d = \cos(0.25\,\mathrm{t})\ \ (\mathrm{m}) \\ z_d = 3 - 2\cos(0.25t)\ \ (\mathrm{m}) \end{cases} \tag{65}$$

The initial position and attitude of the quadrotor are set as $[x(0)\,, y(0)\,, z(0)] = [0,\ \ 0.8,\ \ 0.8](\mathrm{m})$, $[\phi(0), \theta(0), \psi(0)] = [\,0 \quad 0 \quad 0\,](\mathrm{rad})$. The disturbances are given as

$$d_{\xi i} = d_s + d_c + d_w(\mathrm{N})\,,$$
$$d_{\eta i} = 2\sin(\,10t + 50)(\mathrm{N\,m})\,.$$

where $d_s = 5$ at $t = 45\,\mathrm{s}$ represents the parametric variation.

$$d_c = 0.8(\,\sin(0.5t + 50) + \cos(0.5t + 50)),$$

$$d_w = 10\left(\exp\left(-\frac{1}{2}\frac{(t-10)^2}{0.1^2}\right) + \exp\left(-\frac{1}{2}\frac{(t-60)^2}{0.1^2}\right)\right)$$

.

Space circle trajectory tracking results are shown in Figure 21. Position tracking errors are shown in Figures 22 to 24. As shown in Figures 21 to 24, the PID+PID controller achieves good tracking performance. However, the overshoot and the settling time of the PID controller are much larger and longer than those of the APD-SMC+RISE controller. It also can be seen that, before d_s is introduced, the tracking performance of PD-SMC+RISE controller is

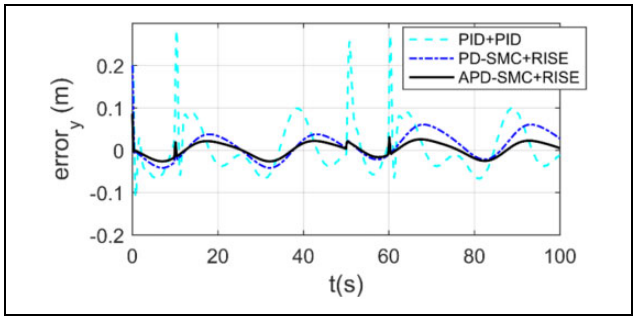

Figure 23. Position tracking error in *y*-axis.

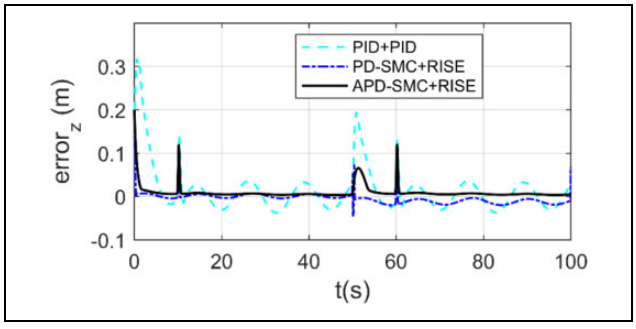

Figure 24. Position tracking error in *z*-axis.

almost as good as that of the APD-SMC+RISE. However, when d_s is introduced at $t = 45$ s, the PD-SMC+RISE controller cannot compensate for it without changing the control gains such that obvious steady-state error appears.

Compared with the PID+PID and PD-SMC+RISE controllers, the APD-SMC+RISE controller has the best tracking performance. As shown in Figures 22 to 24, the overshoot and settling time under the APD-SMC+RISE controller are smaller and shorter than those under the PID+PID controller. Above all, by introducing the adaptive estimations, the APD-SMC+RISE controller achieves adaptive tracking capability and the disturbances have been well compensated with reasonable control gains.

Summing up, the above simulation results have validated that the proposed control strategy could not only track complex trajectories with high accuracy but also have strong robustness against various disturbances.

Conclusions

This article studies the trajectory tracking of a nonlinear underactuated quadrotor UAV and proposes a robust model-free hierarchical controller. On one hand, a robust APD-SMC law is designed for the outer loop to drive the quadrotor track the desired position trajectory with null steady-state errors and the requirement for accurate dynamic model is also avoided. On the other hand, RISE feedback control method is employed in the inner loop for attitude tracking control and disturbance rejection. The proposed controller not only has simple structure but also has strong robustness to various external disturbances. Its effectiveness has been validated by extensive simulation experiments. Further work will focus on validating the proposed control strategy in practical applications.

Declaration of conflicting interests

The author(s) declared no potential conflicts of interest with respect to the research, authorship, and/or publication of this article.

Funding

The author(s) received no financial support for the research, authorship, and/or publication of this article.

ORCID iD

Xin Ma http://orcid.org/0000-0003-4402-1957

References

1. Trasviña-Moreno CA, Blasco R, Marco Á, et al. Unmanned aerial vehicle based wireless sensor network for marine-coastal environment monitoring. *Sensors* 2017; 17(3): 460–482.
2. Naidoo Y, Stopforth R, and Bright G. Development of an UAV for search and rescue applications. In: *IEEE Africon*. Zambia: Livingstone, 2011, pp. 13–15.
3. Wang C, Savkin AV, and Garratt M. A strategy for safe 3D navigation of nonholonomic robots among moving obstacles. *Robotica* 2018; 36(2): 275–297.
4. Kendoul F. Survey of Advances in guidance, navigation, and control of unmanned rotorcraft systems. *J Field Robot* 2012; 29(2): 315–378.
5. Tayebi A and McGilvray S. Attitude stabilization of a VTOL quadrotor aircraft. *IEEE Trans Control Syst Technol* 2006; 14(3): 562–571.
6. Robio JJ. Robust feedback linearization for nonlinear processes control. *TSA Trans* 2018; 74: 155–164.
7. Robio JJ, Pieper J, Meda-Campaña JA, et al. Modeling and regulation of two mechanical systems. *IET Sci Mesure Technol* 2018; 12(5): 657665.
8. Robio JJ, Lopez J, Pacheco J, et al. Control of two electrical plants. *Asian J Control* 2018; 20(5): 1–15.
9. Pounds PEI, Bersak DR, and Dollar AM. Stability of small-scale UAV helicopters and quadrotors with added payload mass under PID control. *Auton Robot* 2012; 33(1–2): 129–142.
10. Panomrattanarug B, Higuchi K, and Mora-Camino F. Attitude control of a quadrotor aircraft using LQR state feedback controller with full order state observer. In: *SICE annual conference*, Nagoya, Japan, 14–17 September 2013, pp. 2041–2046. IEEE Xplore.
11. An HL, Li J, Zhang KK, et al. Backstepping-based inverse optimal attitude control of quadrotor. *Int J Adv Robot Syst* 2016; 85(2): 1281–1295.
12. Chen FY, Lei W, Zhang KK, et al. A novel nonlinear resilient control for a quadrotor UAV via backstepping control and

nonlinear disturbance observer. *Nonlin Dynam* 2016; 85(2): 1281–1295.
13. Derafa L, Benallegue A, and Fridman L. Super twisting control algorithm for the attitude tracking of a four rotors UAV. *J Frankl Inst* 2012; 349(2): 685–699.
14. Xu R and Ozguner U. Sliding mode control of a quadrotor helicopter. In: *Proceedings of IEEE conference on decision and control*, San Diego, 13–15 December 2006, pp. 4957–4962. IEEE Xplore.
15. Zheng EH and Xiong JJ. Quad-rotor unmanned helicopter control via novel robust terminal sliding mode controller and under-actuated system sliding mode controller. *Optik Int J Light Elect Opt* 2014; 125(12): 2817–2825.
16. Gonzalez-Hernandez I, Palacios FM, Cruz SS, et al. Real-time altitude control for a quadrotor helicopter using a super-twisting controller based on high-order sliding mode observer. *Int J Adv Robot Syst* 2017; 14(1): 1–15.
17. Wang J, Geamanu MS, Cela A, et al. Event driven model free control of quadrotor. In: *IEEE International Conference on Control Applications*, Hyderabad, India, 28–30 August 2013, pp. 722–727. IEEE Xplore.
18. Wang HP, Ye XF, Tian Y, et al. Model-free-based terminal SMC of quadrotor attitude and position. *IEEE Trans Aeros Elect Syst* 2016; 52(5): 2519–2528.
19. Dinh TX and Ahn KK. Adaptive tracking control of a quadrotor unmanned vehicle. *Int J Precis Eng Man* 2017; 18(2): 163–173.
20. Pan YP, Liu YQ, Xu B, et al. Hybrid feedback feedforward: an efficient design of adaptive neural network control. *Neural Netwk* 2016; 76: 122–134.
21. Pan YP and Yu HY. Biomimetic hybrid feedback feedforward neural-network learning control. *IEEE Trans Neural Netwk Learn Syst* 2017; 28(6): 1481–1487.
22. Torres F, Rabhi A, Lara D, et al. Fuzzy state feedback for attitude stabilization of quadrotor. *Int J Adv Robot Syst* 2016; 85(1): 1–9.
23. Gautam D and Ha C. Control of a quadrotor using a smart self-tuning fuzzy PID controller. *Int J Adv Robot Syst* 2013; 10: 1–9.
24. Kayacan E and Maslim R. Type-2 fuzzy logic trajectory tracking control of quadrotor VTOL aircraft with elliptic membership functions. *IEEE/ASME Trans Mech* 2017; 22(1): 339–348.
25. Dierks T and Jagannathan S. Output feedback control of a quadrotor UAV using neural networks. *IEEE Trans Neural Netwk* 2010; 21(1): 50–66.
26. Lou WJ and Guo X. Adaptive trajectory tracking control using reinforcement learning for quadrotor. *Int J Adv Robot Syst* 2016; 13(38): 1–10.
27. Chovancová A, Fico T, Chovanec Ľ, et al. Mathematical modelling and parameter identification of quadrotor (a survey). *Proc Eng* 2014; 96: 172–181.
28. Slotine JJE and Li WP. *Applied nonlinear control*. Englewood, Cliffs: Prentice-Hall Press, 1991.
29. Xian B, Dawson DM, Queiroz MSD, et al. A continuous asymptotic tracking control strategy for uncertain nonlinear systems. *IEEE Trans Autom Control* 2004; 49(7): 1206–1211.
30. Ouyang PR, Acob J, and Pano V. PD with sliding mode control for trajectory tracking of robotic system. *Robot Cim Int Manuf* 2014; 30(2): 189–200.
31. Ouyang PR, Pano V, and Hu YQ. Position domain PD sliding mode control for contour tracking. In: *IEEE international conference on advanced intelligent mecharonics*, Busan, 7–11 July 2015, pp. 1020–1025. IEEE Xplore.
32. Bo Z, Bin X, Yao Z, et al. Nonlinear robust adaptive tracking control of a quadrotor UAV via immersion and invariance methodology. *IEEE Trans Indus Elect* 2015; 62(5): 2891–2902.
33. Shin J, Kim HJ, Kin Y, et al. Autonomous flight of the rotorcraft-based UAV using RISE feedback and NN feedforward terms. *IEEE Trans Control Syst Technol* 2012; 20(5): 1392–1399.
34. Yue WH, Pano V, Ouyang PR, et al. Model-independent position domain sliding mode control for contour tracking of robotic manipulator. *Int J Syst Sci* 2017; 48(1): 190–199.
35. Mahony R, Kumar V, and Corke P. Multirotor aerial vehicles: modeling, estimation, and control of quadrotor. *IEEE Robot Autom Magaz* 2012; 19(3): 20–32.
36. Naidoo Y, Stopforth R, and Bright G. Quad-rotor unmanned aerial vehicle helicopter modelling and control. *Int J Adv Robot Syst* 2011; 8(4): 139–149.
37. Khatoon S, Nasiruddin I, and Shahid M. Design and simulation of a hybrid PD-ANFIS controller for attitude tracking control of a quadrotor UAV. *Arab J Sci Eng* 2017; 42(12): 5211–5229.
38. Raffo GV, Ortega MG, and Rubio FR. An integral predictive/nonlinear H∞ control structure for a quadrotor helicopter. *Automatica* 2010; 46(1): 29–39.
39. Boudjedir H, Bouhali O, and Rizoug N. Adaptive neural network control based on neural observer for quadrotor unmanned aerial vehicle. *Adv Robot* 2014; 28(17): 1151–1164.
40. Boyd S and Vandenberghe L. *Convex optimization*. Cambridge: Cambridge Univ. Press, 2004.
41. Altuğ E, Ostrowski JP, and Taylor CJ. Control of a quadrotor helicopter using dual camera visual feedback. *Int J Robot Res* 2015; 24: 329–341.
42. Chamseddine A, Zhang Y, Rabbath CA, et al. A flatness-based trajectory planning/replanning for a quadrotor unmanned aerial vehicle. *IEEE Trans Aeros Elec Syst* 2012; 48(4): 2832–2848.
43. Han J. From PID to active disturbance rejection control. *IEEE Trans Indus Elect* 2009; 56(3): 900–906.